MODELING THE ORIENTATIONAL AND POSITIONAL BEHAVIOR OF POLYHEDRAL NANOPARTICLES AT FLUID-FLUID INTERFACES

A Thesis

Presented to the Faculty of the Graduate School

of Cornell University

In Partial Fulfillment of the Requirements for the Degree of

Master of Science

by

Unmukt Gupta

January 2017

© 2017 Unmukt Gupta

ABSTRACT

Using Molecular Dynamics simulations to explicitly model fluid molecules, we study the effect of solvent wetting on the behavior of polyhedral nanoparticles at a fluid-fluid interface. First, we quantify the positional and orientational free energy characteristics of an isolated nanoparticle. Our results suggest that the thickness of the interface can introduce non-trivial effects on the preferential particle orientations. A continuum model is proposed to account for the finite interfacial mixing region, and a qualitative comparison between the two approaches is presented. We examine the effect on the free energy of the system of changes in the particle's solvation preference towards one fluid, and the degree of miscibility between the two fluids. By tuning these interaction parameters, we can potentially access and favor different orientations for the particle shapes examined. Further, we extend the insights gained from single particle analyses to the attachment of two particles. Our results reveal conditions that can drive the assembly of Cuboctahedra into either 2D Puckered Honeycomb lattices or linear rod-like structures.

BIOGRAPHICAL SKETCH

Unmukt Gupta was born in New Delhi, India in the year 1992. After completing his schooling in the year 2010, he joined the Indian Institute of Technology (IIT), Delhi for an undergraduate degree in Chemical Engineering. In the summer of 2012, he had the opportunity to do a research internship at Prof. George Whitesides' lab at Harvard University. Through this internship, that lasted for 4 months, he gained experience in the field of "Soft Robotics". He co-authored two journal articles in the process based on the findings that detail the results of the research.

After completing his undergraduate degree in 2014, he joined Prof. Fernando A. Escobedo's lab in the department of Chemical and Biomolecular Engineering (CBE) at Cornell University to pursue a Master of Science degree. Under Prof. Escobedo's guidance, he worked on modeling the self-assembly of colloidal Nanoparticles at fluid-fluid interfaces as part of his master's thesis. After being admitted to the Ph.D. program, he will continue his research starting Fall 2017.

ACKNOWLEDGEMENTS

I would like to express my gratitude to my advisor, Prof. Fernando A. Escobedo from the department of Chemical and Biomolecular Engineering, Cornell University, for his constant guidance and support throughout the duration of this project. I would like to thank Prof. Tobias Hanrath for helping me gain insight into the experimental aspects of this research, and Prof. Paul H. Steen for useful exchanges.

I am also grateful to Dr. Vikram Thapar for insightful discussions through the course of this project. Lastly, I would like to acknowledge funding support from a SEED Grant provided by NSF MRSEC award to Cornell, Grant DMR-1120296.

TABLE OF CONTENTS

I. INTRODUCTION

With the recent advances in the synthesis of Quantum Dot Nanoparticles (NP), we are gradually stepping into a new paradigm of material synthesis, wherein we can tailor the design of a NP superstructure by controlling the assembly of these nano-sized building blocks, and in doing so, tailor the material's properties. One of most commonly used approach to control the self-assembly of NPs is to restrict the motion of the NPs to two dimensions, e.g., by depositing them on a flat solid substrate or by pinning them at a fluid-fluid interface. Numerous experimental efforts[1]-[5] have been made over the years to increase the repeatability, precision and control over the self-assembly of colloidal NPs into quasi-2D superstructures with programmable symmetry. In recent years, these quasi-2D superstructures have found multiple technologically important applications; e.g. in optics[6]-[8], photovoltaics[9]-[11], and catalysis[12], [13].

The self-assembly of NPs at a fluid-fluid interface is driven by a complex interplay of entropic and enthalpic forces. Although simulation studies have mostly focused on investigating systems dominated by entropic effects through Monte Carlo simulations of hard-core particles[14]-[17], a few studies have also examined systems exhibiting enthalpic interactions using Molecular Dynamics (MD) simulations[18], [19]. The current work primarily aims to assess the role of enthalpic interactions on the self-assembly process, through the use of a coarse-grained model for the polyhedral NPs and explicit molecules to describe the fluids. The use of polybead models to represent polyhedral objects facilitates not only the implementation of enthalpic interactions but

also the use of MD simulations which conveniently exploit multi-processor computing capabilities.

It has been long known that colloidal NPs possess a strong affinity towards fluid-fluid interfaces and can bind to them irreversibly[20], [21]. It is widely believed that the driving force behind this irreversible adsorption is the reduction in the interfacial energy due to contact between the two immiscible fluids. Based on this principle, many analytical models[2]-[4], [22]-[24] have been developed to capture the orientational behavior of isolated NPs at sharp (zero thickness) fluid-fluid interfaces. For example, Evers et al. [2] predict that the most preferred orientation of a cubic NP at the interface is {110} facet up. While most suitable for applications to particle at micron size scales, the effect of an interfacial region with a finite “thickness” cannot be neglected when nano-scale particles are involved.

We seek to establish the underlying thermodynamic principles governing the self-assembly of NPs using flat (fluid) interfaces as templates. The first step in this process is to investigate the behavior of an isolated NP at the interface. For this purpose, we use both particle-based coarse-grained molecular simulation and a theoretical continuum model. Specifically, we employ solvent-explicit MD simulations to simulate the multibody effect of the fluid molecules on the NP. By explicitly modeling the interface, the effect of solvent wetting characteristics on the NP behavior can be more accurately captured. We use these simulations to map out the free-energy of the NPs as a function of their orientations and vertical positions with respect to the interface,

and thus to identify the preferred particle configurations. We use selected molecular simulation results for a cube shape to illustrate the basis of the general characteristics displayed by an isolated NP at the interface, and to motivate the development of our continuum model where an interfacial region of finite thickness contributes explicitly to the free energy of the system.

The rest of this manuscript is organized as follows. In section II we describe the coarse-grained simulation model and simulation methodology. In section III we summarize the basis of our continuum model (providing additional details in the Appendix). In section IV we present the main results for a single NP near an interface, comparing key simulation data and trends to those predicted by the continuum model. In that section, we also extend the principles developed for a single NP to explain the assembly of two-particle systems (simulating polybead Cuboctahedra as test bed). In section V we close with some concluding remarks and an outline of suggested future work.

II. MODELS AND METHODS

2.1 Coarse-grained model and molecular dynamics (MD)

The base system consists of a single colloidal NP, suspended at the interface of two vertically-stacked immiscible fluids (two NPs are simulated in select cases). For simplicity, the direction perpendicular to the average orientation of the interface is, henceforth, referred to as the vertical direction (represented by the y-axis). By construction, the interface is initially located at the center of the simulation box. The interface location is maintained near the box center by adding reflective walls at the box edges perpendicular to the vertical direction. Periodic boundary conditions (PBCs) are imposed in the x and z directions. For a single NP system, the typical simulation box size is $20\times40\times20\sigma^3$ (in the X-Y-Z dimensions respectively).

The Nanoparticles are described using a *Polybead model* [25]. The desired shape is carved out from a Cubic Close Packed lattice, wherein each face is represented by a well-defined crystallographic plane. The NP is then shaped by placing Lennard-Jones beads at the surface/outermost lattice sites only. The surrounding liquids (solvent and sub-phase) are explicitly defined as dimers of LJ beads. While such dimers are intended to be a coarse-grained representation of the fluid molecules, they are able to capture the multibody forces associated with the wetting characteristics of NPs and the varying fluid properties across the fluid-fluid interface. Typically, the number of solvent molecules was around 5500.

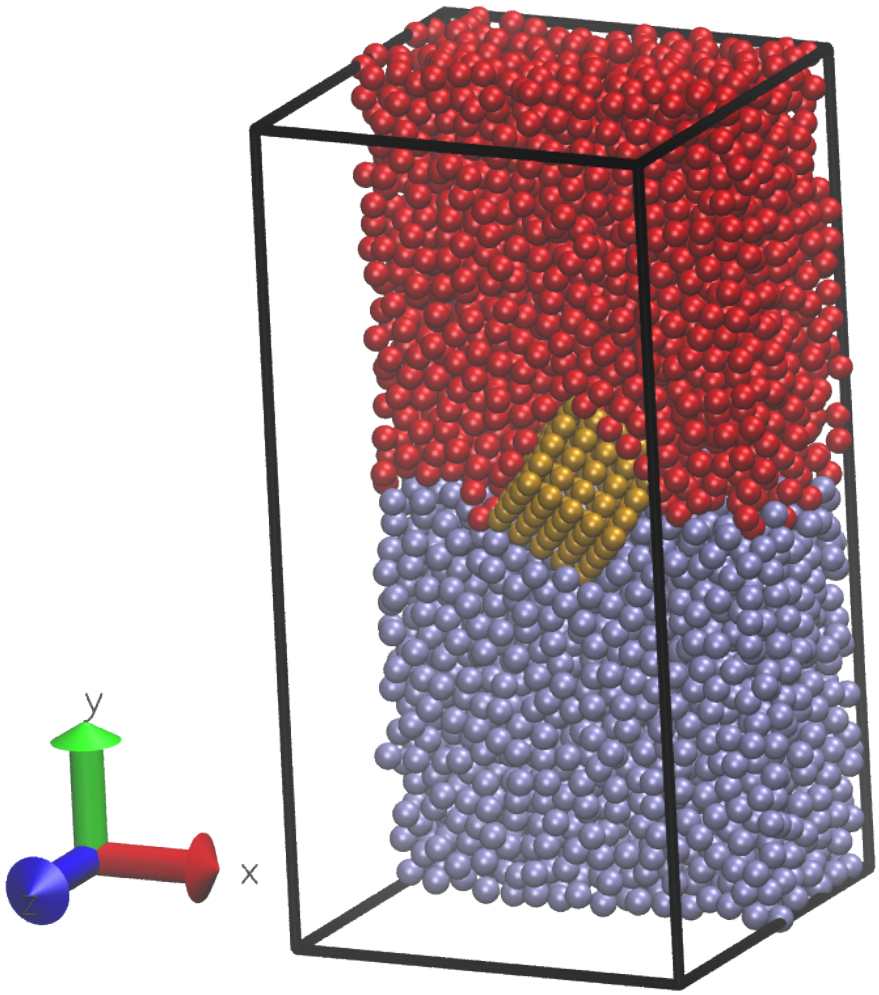

Figure 1: Snapshot of the polybead model depicting two fluid phases (in red and blue) and a cubic NP (in yellow) at their interface. For the sake of visibility, fluid molecules have been removed from the front half of the simulation box.

The interaction between any two species is modeled by tuning the interactions between their corresponding beads. This inter-bead interaction is defined by the (12-6) cut and linearly shifted Lennard-Jones potential,

$$U(r_{ij}) = \phi(r_{ij}) - \phi(r_c) - (r_{ij} - r_c)\left.\frac{d\phi}{dr_{ij}}\right|_{r_{ij}=r_c} ; r_{ij} < r_c \quad (1)$$

$$\phi(r_{ij}) = 4\varepsilon_{ij}\left[\left(\frac{\sigma}{r_{ij}}\right)^{12} - \left(\frac{\sigma}{r_{ij}}\right)^{6}\right] \quad (2)$$

where r_{ij} is the distance between beads *i* and *j* and the cutoff radius is $r_c = 2.5$. The effective diameter (σ) of all beads (in the NP and the two liquids) is taken to be the same ($\sigma = 1.0$). The bond in a liquid dimer is described by the FENE potential,

$$U(r) = -0.5KR_0^2\, ln\left[1 - \left(\frac{r}{R_0}\right)^2\right] + 4\epsilon\left[\left(\frac{\sigma}{r}\right)^{12} - \left(\frac{\sigma}{r}\right)^{6}\right] + \epsilon \quad (3)$$

and the bond length is maintained at 1σ ($K=30\varepsilon/\sigma^2$, $R_0=1.5\sigma$). MD simulations are performed using the canonical (NVT) ensemble in LAMMPS[26]. The simulation temperature is maintained at $0.85\varepsilon/k_B$ using the Nosé-Hoover Thermostat. In this work, we only consider systems with a liquid-liquid interface, and so the density is kept close to 0.8 beads/σ^3, and the integration step is 0.005τ. Typical values of the reduced parameters for comparison with experimental data, as reported in ref. [27], are σ = 0.3nm, $\varepsilon = 100k_B$, and τ = 2ps.

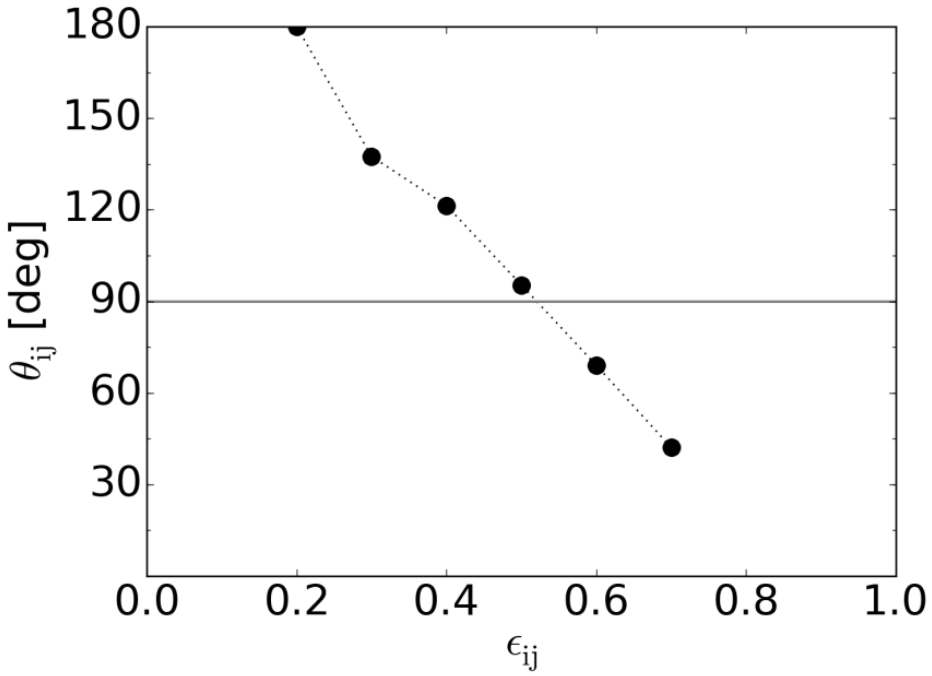

Figure 2: Calibration of intrinsic wetting angle, θ_{ij}, with the solid-fluid LJ energy parameter ε_{ij}.

Using the method given by Savoy et al.[28] , the LJ well depth parameter (ε_{ij}) is tuned to correspond to a physically relevant contact angle value (θ_{ij}). In this method a small liquid drop is equilibrated on a flat solid surface (with beads on a square and hexagonal lattice, akin to those on a NP) and the angle θ_{ij} measured directly. The resulting calibration curve is shown in Figure 2. The degree of miscibility between the two fluids is determined by the value of $\varepsilon_{S1,S2}$. For all the systems in the following sections, we first establish a base case where the ε_{ij} value between all species is set to 0.5. This ensures that the NP interacts symmetrically with both the fluids, and the respective contact angle values are close to 90˚.

2.2 Free energy (FE) and key degrees of freedom

The microstate of a single NP (and the free energy associated with it) is fully determined by its position and orientation relative to the fluid-fluid interface. We use a vertical position (H) and Euler angles (θ, ψ) to describe such degrees of freedom.

The interface diving surface is defined as the plane parallel to the average orientation of the interface and dividing the finite interface symmetrically through the middle. The distance H from the NP center of mass (COM) to the interface dividing plane is referred to as “vertical” position and is given in reduced units “y/e” where e is the edge length or a characteristic size parameter of the NP. In order to quantitatively characterize the thermodynamic driving force that controls the vertical position (H) of the NP, we perform Umbrella Sampling [29] simulations to estimate the underlying Free energy (FE) profile. For this purpose, we divide the vertical position space into overlapping windows and use a harmonic biasing potential to constrain the NP to each window. A Weighted Histogram Analysis Method (WHAM)[30] scheme is then used to combine the results from individual simulation windows into the final unbiased FE profile.

Particle orientation is represented using the intrinsic Euler angle convention (y-z’-y’’) with three angles (φ, θ, ψ). The elemental rotations occur about the axes of the local coordinate system (fixed to the particle). Angle φ gives the rotation about the y-axis, i.e. the axis perpendicular to the interface. Rotation about this axis does not change the NP configuration with respect to the interface, and hence we ignore it. The tilt

angle, θ described the rotation about the new (rotated in step 1) z-axis, and the spin angle, ψ gives the rotation about the new (rotated in step 2) y-axis.

For an isolated NP (of a given shape and size) at the interface, a free energy landscape can be generated with tilt (θ) and spin (ψ) angles as parameters using an Umbrella Sampling technique. The vertical position of the NP is decoupled from such calculation by allowing it freely fluctuate around its equilibrium position. The 2D orientation phase space is divided into overlapping windows. Independent MD simulations are run for each window with two discrete harmonic torsion springs constraining the corresponding orientation angles. The windows are then stitched together using WHAM to generate the unbiased FE landscape. The minima in this landscape helps identify the orientation preference of the NP.

III. THEORETICAL MODEL: CONTINUUM APPROXIMATION

Although the "sharp-interface" theoretical model given by de Graaf et al. has found some success in capturing the preferential orientational preference in certain interfacial systems[31], as it will be shown later in Sec. IV, we find that the predictions of such a theory are inconsistent with our explicit-solvent, cubic-polybead simulation results for the most probable NP orientation and for the FE trends as a function of H. Choi et al.[32] reported that cubic NPs at a fluid-fluid interface orient with the {111} facet up.

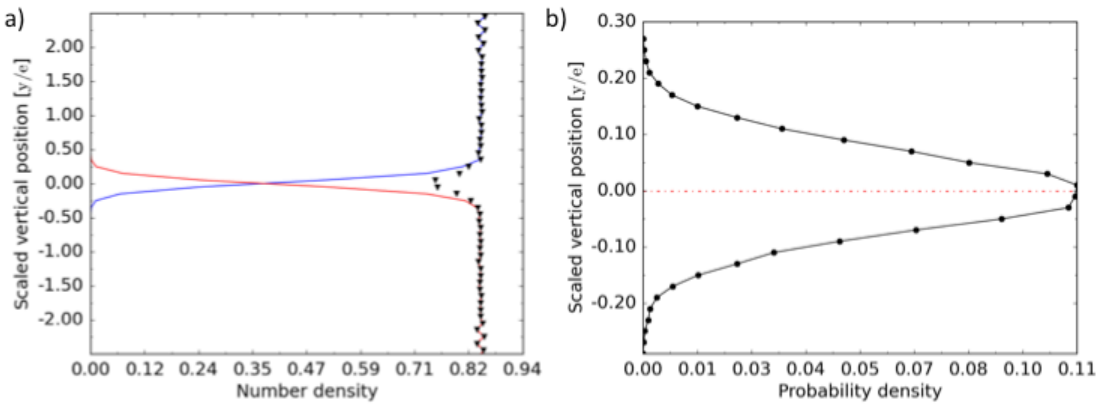

Figure 3: Key properties of fluid-fluid interface. (a) Bead number densities [$1/\sigma^3$] of the bottom fluid (red), top fluid (blue), and of fluid beads (black triangles). (b) Probability density of an unconstrained polybead cube ($e=5\sigma$) at the interface.

One major assumption of the existing theoretical model is the definition of the interface as a plane. However, in reality, the two fluids are not completely immiscible and they partially mix over a finite region[33]. To demonstrate this, we simulated the two

vertically stacked fluids using a long MD run and plotted the density of the fluid "beads" as a function of H (see Figure 3.a). It should be noted that, in this case, the contact angle, $\varepsilon_{S1,S2}$ is set to 0.5. The density of the bottom fluid (red curve) gradually decreases, while that of the top fluid (blue curve) gradually increases as we increase H over a small region from -1.5σ to 1.5σ. We henceforth refer to this region as the mixing region and the width of this region is approximately 3σ. It can be seen that the overall density of the fluid beads (black triangles in Figure 3.a.) decreases in the mixing region. This low density region arises from the unfavorable contact between the two types of fluid beads, which is captured by a low value of $\varepsilon_{S1,S2}$ (= 0.5), and further leads to the low miscibility between the two fluids.

Moreover, the sharp interface model has the implicit assumption of the NP being pinned to a planar interface. As mentioned earlier, the size of the solvent molecules is not negligible compared to the size of a NP. By virtue of thermal energy, (the vertical position of) such a small NP fluctuates significantly about the interface-dividing plane. Figure 3.b shows the probability distribution of a cubic NP as a function of vertical position where the standard deviation about the mean (the interface-dividing plane) is approximately 0.07e (or 0.35σ).

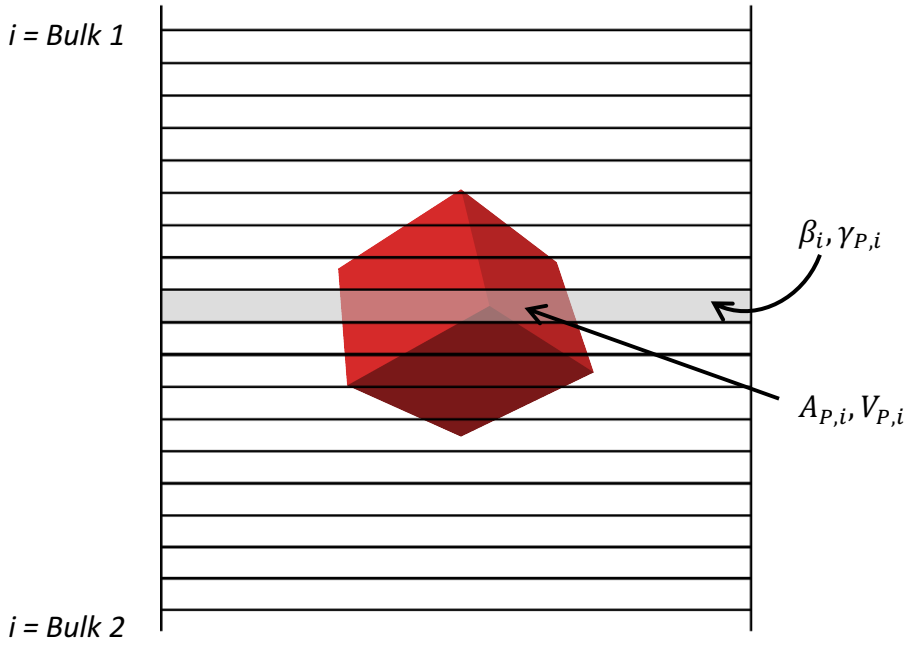

Figure 4: Representation of the theoretical model describing the division of the system into vertical slabs.

To account for these discrepancies, we propose an alternate formulation of the theoretical model where we explicitly account for the contribution of the mixing region to the total energy of the system. We divide the fluid system into a large number of adjacently placed, vertical slabs (see Figure 4). The total potential energy of the system is given as the sum of contributions by each slab. The function is shifted such that the energy of a NP completely immersed in the bulk of fluid 2 is zero:

$$\Delta F(H,\theta,\psi) = \sum_{i=Bulk\ 1}^{Bulk\ 2}\left(\gamma_{P,i} - \gamma_{P,\ Bulk2}\right)A_{P,i} + (\beta_{Bulk\ 2} - \beta_i)V_{P,i} \qquad (4)$$

where $\gamma_{P,i}$ is the interfacial tension between the NP and the fluid phase in the slab, and, β_i is the internal energy per unit volume of fluid phase in the slab. $A_{P,i}$ and $V_{P,i}$ represent the lateral surface area and the volume of NP in the slab, respectively, and V_i represents the total slab volume. Since the interface (mixing region) is a region of unfavorable contact between immiscible solvents, the NP attempts to minimize the volume of the "unfavorable interfacial contact" by maximizing the volume it occupies inside the mixing region. Essentially, the variational principle of finding the values of H, θ, and ψ that minimize the system energy translates now to minimizing the volume of contact, as opposed to minimizing the planar area of contact. Further details on the minimization procedure are outlined in the Appendix

IV. RESULTS AND DISCUSSION

4.1 Single cubic particle at the interface

Figure 5.a shows the underlying FE profile as a function of the vertical height, leaving the particle orientation unconstrained. It can be seen that a cube of edge size, $e=5\sigma$, pays a penalty of ~10 k_BT to move ~0.3e away from the interface-dividing plane. It is clear from the underlying FE profile that the NP can only reside in a small region near the interface (see Figure 3.b).

Figure 5.b shows the FE landscape obtained from US calculations with θ and ψ as parameters (which probe all possible orientations of a cubic NP), while allowing the particle to freely fluctuate perpendicular to the interface. For this "base" case, the contact angle between the NP and both fluids was ~90˚ (i.e., $\varepsilon_{S1,NP} = \varepsilon_{S2,NP} = \varepsilon_{S1,S2} = 0.5$). It is observed that the cubic NP exhibits the strongest preference for the {111} facet up configuration (see Figure 5.c), while the smallest preference for the {100} facet up configuration.

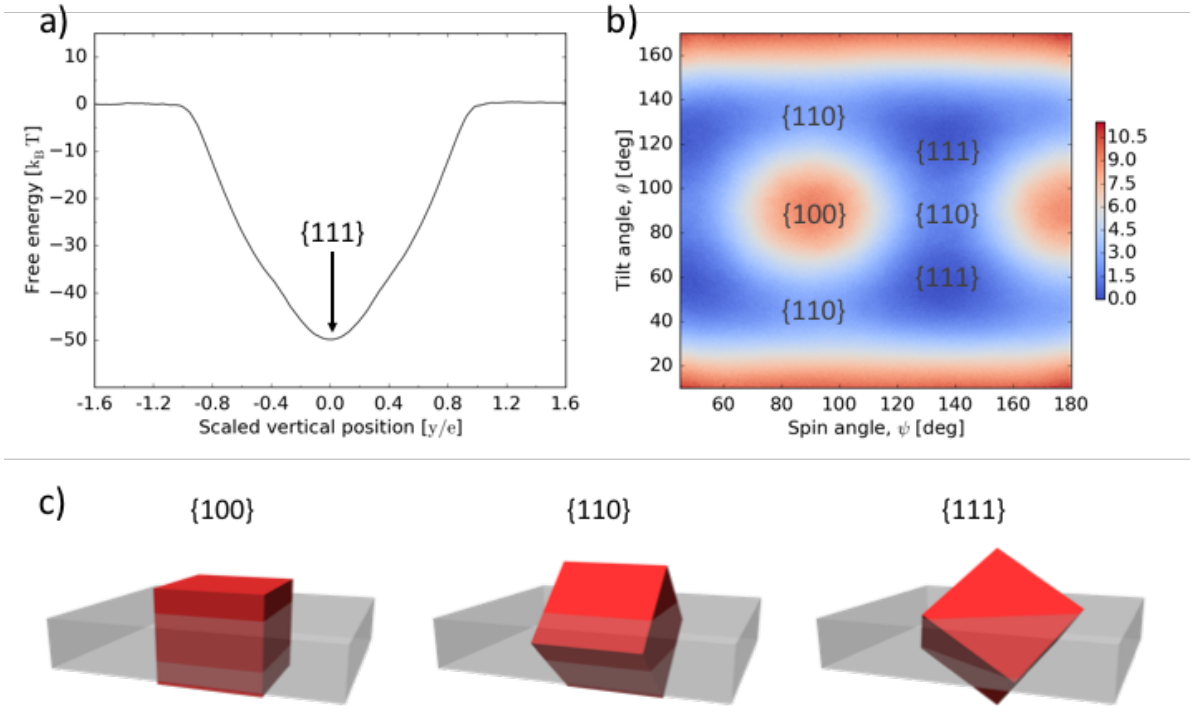

Figure 5: a) FE as a function of H for a polybead cube (e=5σ) at base case conditions. The most preferred orientation is {111} up near the interface-dividing plane. b) Orientational FE landscape for cube (e=5σ) marked with the locations of {100}, {110}, and {111} up orientations (scale bar in k_BT units). c) Depiction of the {100}, {110}, and {111} up orientations of the cube, with the grey region representing the finite interfacial mixing region (for simplicity, the polybead cube is shown as a perfect cube).

In general, it was observed that pinning the NP at different vertical positions (H) causes a change in the orientational behavior. It is possible to break down the FE landscape along the NP vertical position into independent contributions from various orientational configurations. To do this, we fixed the θ and ψ angles of the NP, and performed a 1D US calculation (similar to that described in section 2.2) with the vertical position as the

only parameter. Figure 6.a shows these results for a polybead cube of size 5σ where, for any vertical position, the orientation with the lowest free energy would be expected to be most stable. An alternate way to interpret this behavior is by envisioning that the NP is free to rotate and the 3 orientations considered are the most important ones; then the unconstrained vertical FE landscape is the lowermost envelope of all such possible curves. Each point in said envelope corresponds to the most stable orientation (lowest FE) at that vertical position.

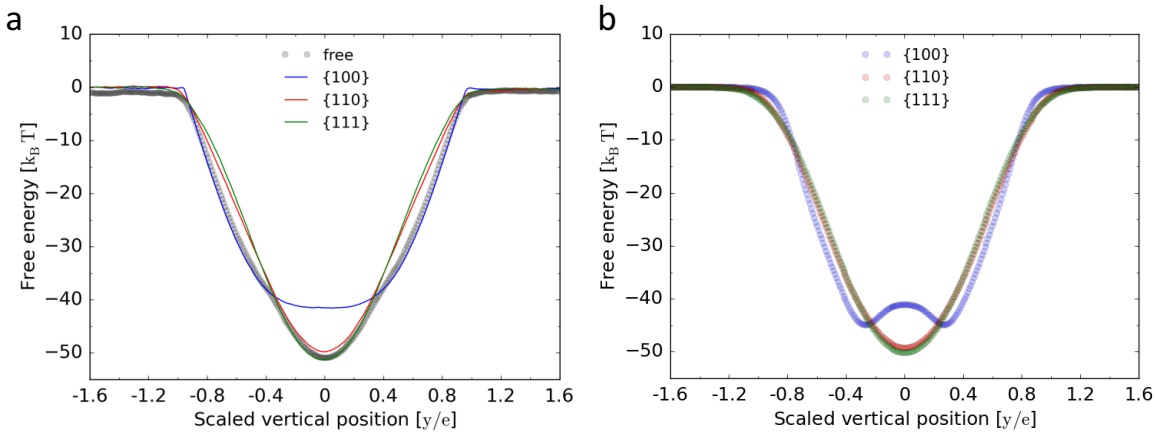

Figure 6: FE vs H for a cube at the base case conditions corresponding to three major orientations (blue, red, and green) and for the most stable orientation envelope (black). (a) Polybead model with e = 5σ; (b) Continuum model.

It can be seen (in Figure 6.a.) that the FE of the {111} facet up orientation is lower than that of {110} facet up. case, the {100} facet up configuration is stable beyond a certain distance from the interface-dividing plane (Figure 6.a). This {111}-up to {100}-up change in preferential orientation is characterized by a slight flattening of the FE

profile, followed by a change in its slope. These characteristics are correctly predicted by our version of the continuum model as seen in Figure 6.b.

4.2 Tuning orientation preference of NP by changing relative contact angles

For practical applications, it is important to understand how the interfacial properties of the fluids and the particle affect the preferential orientation that an isolated NP will exhibit at the fluid-fluid interface. We show here how different such NP orientations can be accessed and favored, by tuning the relative contact angle parameters. In particular, we consider two cases:

i. Changing $\varepsilon_{S1,S2}$ – the degree of miscibility between the two solvents: Increasing $\varepsilon_{S1,S2}$ increases the miscibility of the two fluids and, to some degree, leads to an increase in the width of the mixing region. For a higher value of $\varepsilon_{S1,S2}$, we observed a relatively shallower free energy profile (see Figure 7) along the vertical position. This result is consistent with the predictions from the continuum model since if the fluids are more miscible, the energy per unit volume (β_i) in the mixing region is relatively lower. As per Eq. (4), a smaller negative value of the prefactor ($\beta_{Bulk\ 2} - \beta_i$) for the excluded volume term ($V_{P,i}$) will give a shallower FE profile.

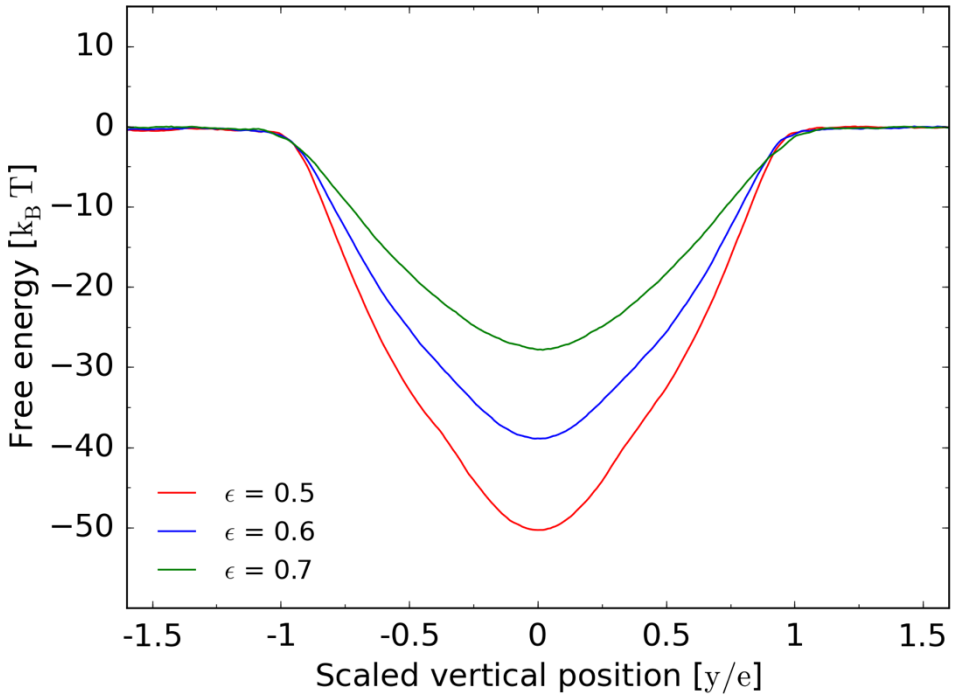

Figure 7: FE profile for a cube (e=5σ) for different values of $\varepsilon_{S1,S2}$ (keeping $\varepsilon_{NP,S1}$=$\varepsilon_{NP,S2}$=0.5 constant). Higher values of $\varepsilon_{S1,S2}$ generate successively shallower wells.

A shallower FE well allows the NP to symmetrically access higher vertical positions by virtue of its thermal energy. Interestingly, the ratio of any two FE profiles (for symmetric fluids, with FE shifted to zero for large H), corresponding to different values of $\varepsilon_{S1,S2}$, is a constant. The values for this ratio are approximately 1.3 for $\varepsilon_{S1,S2}$ = 0.6, and 1.8 for $\varepsilon_{S1,S2}$ = 0.7.

ii. Changing $\theta_{NP,S}$ – the contact angles between solvents and the NP: By decreasing $\theta_{NP,S1}$ (i.e., increasing $\varepsilon_{NP,S1}$), we give the particle an enthalpic preference to solvent 1 relative to solvent 2 and thus an incentive to move away

from the interface-dividing plane. As shown in Figure 8.a, this change expectedly shifts the global minimum of the vertical FE profile to a higher H=H*, effectively changing the particle's mean position from 0.0 to H*. From the continuum perspective, due to the lower energy of interactions between NP and fluid 1, fluid slabs with a higher concentration of fluid 1 have a lower value of $\gamma_{P,i}$. Thus, the FE in the bulk of fluid 1 is lower than that in the bulk of fluid 2.

For $\varepsilon_{NP,S1}$=0.7, we see a change in the preferred orientation of the NP from {111} to {100} (Figure 8.c). But, we also see that the depth of the orientational bias well is small (~3 k_BT).

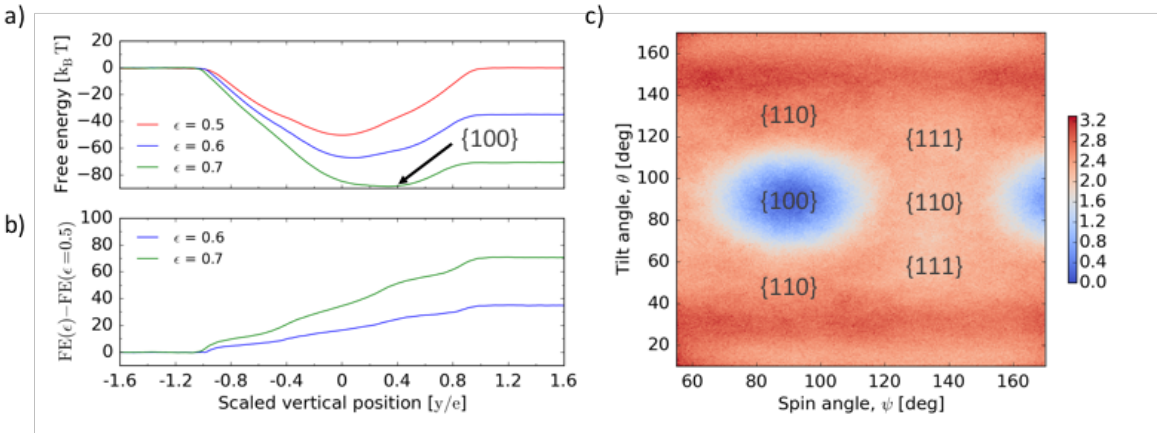

Figure 8: (a) FE vs H for a cube (e=5σ) for different values of $\varepsilon_{NP,S1}$ (keeping $\varepsilon_{S1,S2}$=0.5 constant); (b) Difference in FE (ΔF) between the profiles corresponding to higher $\varepsilon_{NP,S1}$ and the base case ($\theta_{NP,S1}$ = 0.5). (c) Orientational FE landscape for a cube (e=5σ) marked with the locations of {100}, {110}, and {111}-up orientations with $\theta_{NP,S1}$ = 0.7 and $\varepsilon_{S1,S2}$=0.5.

As shown in Figure 8.a, for specific values of $\theta_{NP,S1}$, the vertical FE profile is effectively flattened over a large range of positive H values (green curve). In such a situation, the NP can reside over a wide range of vertical positions with almost equal probability, and effectively experiences minimal orientational and positional preference. A multi-particle self-assembly process under these conditions would hence be expected to be dominated by entropic (packing) forces and NP-NP interactions.

Finally, another approach to tune NP orientation involves modifying both $\varepsilon_{S1,S2}$ and $\theta_{S1,NP}$ synergistically to gain a finer control over the shape of the FE profile. We can see from Figure 9 that for $\varepsilon_{S1,NP}$=0.7 and $\varepsilon_{S1,S2}$=0.6, for a cube of 5σ size, the FE minima is shifted from H=0.0 to H=1.5σ, without flattening the profile. In this manner we retain the positional selectivity while accessing a different preferential NP orientation (namely, {100} facet up).

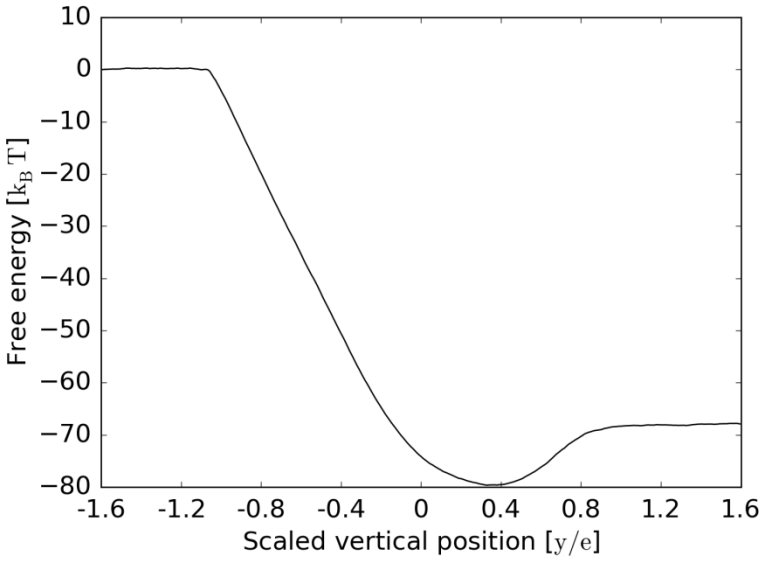

Figure 9: FE vs H for a cube (e=5σ) with $\varepsilon_{S1,S2}$=0.6, $\varepsilon_{NP,S1}$=0.7; the cube's most preferred position shifts upwards to ~0.4e, and its most preferred orientation changes from {111} to {100} facet up.

4.3 Assembly of two particles at the interface

Toward a future goal of describing multi NP interfacial assembly, we attempt here to explain two-particle behavior at the interface as an extension to the previous insights already gained on single particle behavior in Sec. 4.1 and 4.2. As it will be shown, two-particle interfacial assembly can be explained by the interplay of the underlying FE characteristics for individual NPs at the interface and the FE associated with NP-NP interactions. For this purpose, we choose to illustrate our analysis using cuboctahedra (CO) whose particle-particle interactions are richer than those of cubes given that the former can contact each other through two different types of facets.

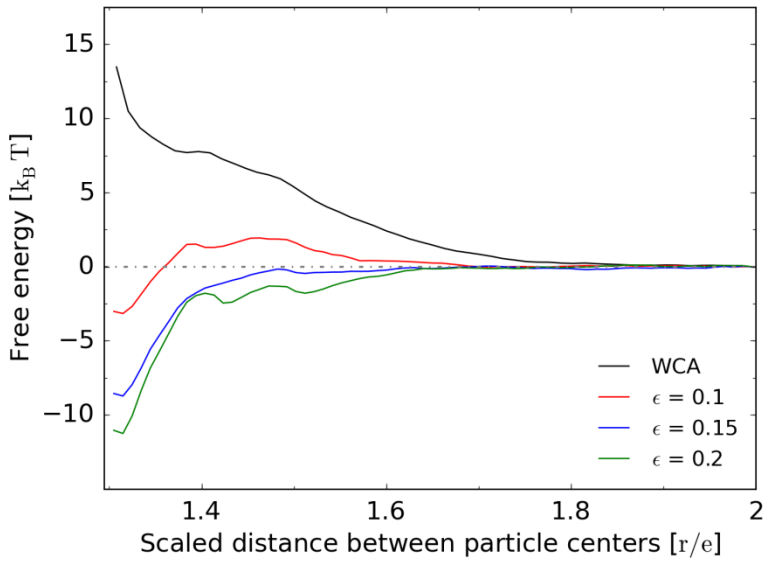

Figure 10: FE of interaction between two COs as a function of the distance between their centers (r), for various values of $\varepsilon_{NP,NP}$ and for purely repulsive NP-NP beads (WCA).

To model NP-NP interactions, we also need to specify the interaction parameter $\varepsilon_{NP,NP}$ between two Lennard-Jones beads belonging to the two different NPs. For a given value of $\varepsilon_{NP,NP}$, it is possible to map the change in FE as a function of the distance between two NPs using umbrella sampling (by adding a biasing harmonic potential between the two NP COMs) and WHAM in a similar way as described in Sec. 2.2. We illustrate one such calculation for two identical COs (e=5σ) in Figure 10, where all other contact angles correspond to ~90˚. For purely repulsive interactions (WCA [34]), the COs are seen to be solvated by a layer of liquid between their contacting surfaces. This is reflected in the increasing trend in FE with decreasing inter-particle distance (i.e., a penalty is incurred in squeezing the liquid layer out). When $\varepsilon_{NP,NP}$ is increased

to 0.15, we begin to see a decreasing FE trend. The closest distance of approach between the centers two COs (from purely geometrical arguments) is $\sqrt{2}e$ (in the case of a square-square facet contact). However, the results of our simulations indicate that the COs come closer than this distance. This is because the bumpy topography of the polybead model causes the two surfaces to contact with a close-packed stacking. We also notice two significant dips in the FE profile for $\varepsilon_{NP,NP}$=0.2. These dips are caused by an intermediate contact between the triangle-triangle facets and the square-triangle facets of the two COs. By synergistically selecting appropriate values of $\varepsilon_{NP,NP}$ and $\varepsilon_{NP,S1}$, one can potentially calibrate the inter-particle attraction to mimic experimental behavior.

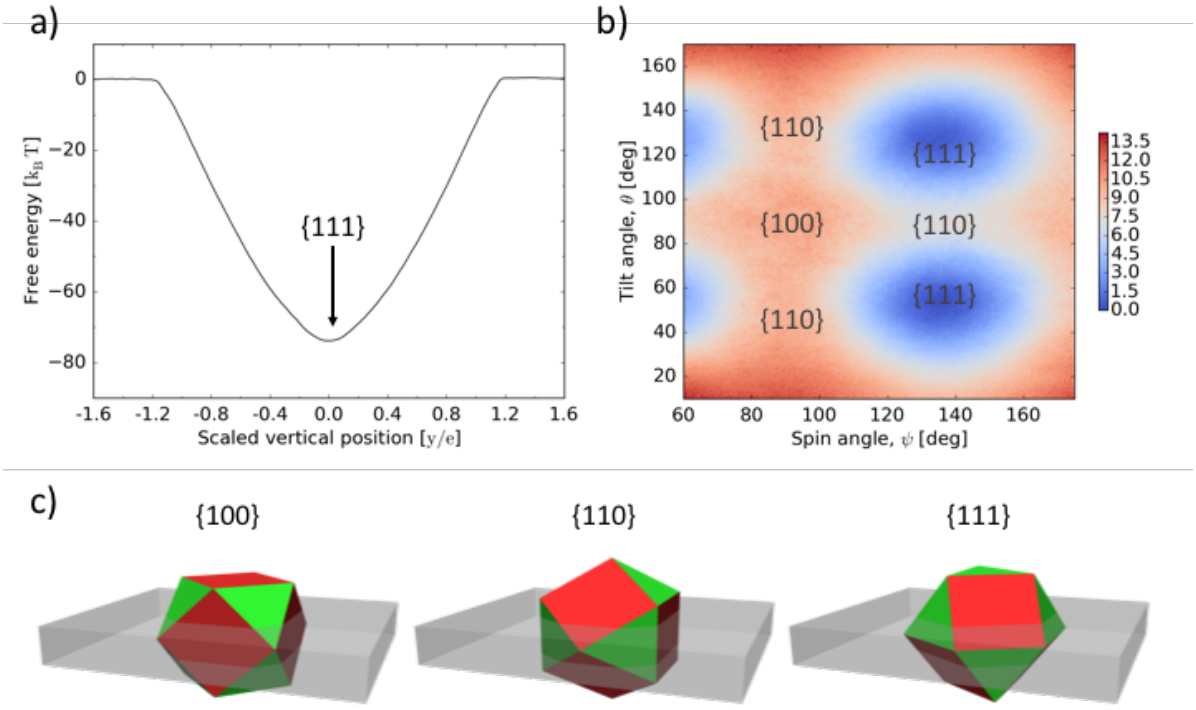

Figure 11: a) FE as a function of H for a polybead CO (e=5σ) for the base case. The most preferred orientation is {111} up near the interface-dividing plane. b) Orientational FE landscape for CO (e=5σ) marked with the locations of {100}, {110}, and {111} up orientations (scale bar in k_BT units). c) Snapshots depicting the {100}, {110}, and {111} orientations of the CO shape, with the grey region representing the finite mixing region.

As dictated by its FE characteristics (see Figure 11), for the base case with all contact angles approximately equal to 90˚ an isolated CO prefers to stay close to the interface-dividing plane while orienting with its {111} facet up. However, as soon as two Cuboctahedra join at the square {100} facet, an additional constraint is added to the system. Now, it is geometrically impossible for both COs to individually satisfy all three

(positional, orientational, contact) constraints simultaneously. If we assume a situation wherein the inter-particle attraction is strong enough to force a complete (square-square) contact constraint, the system now faces the following choices:

1) If the COs remain close to the interface-dividing plane, they can either orient with their {100} facets up to form a square motif or they can orient with their {110} facets up to form a linear rod-like motif. In both of these situations, the CO particles pay an orientational FE penalty, or

2) If the COs attempt to orient in the desired {111} facet up orientation, a vertical distance separates their centers, as seen in Figure 12.a. In this case, they pay a penalty for moving up in the positional FE well. Moreover, if the particles move too far away from the interface-dividing plane, their orientation preference changes from {111} facet up to {110} facet up.

Depending on the specific values of the characterizing parameters ($\theta_{NP,S}$, size of the CO etc.), the system finds a preferred configuration that constitutes a compromise between the competing constraints. For $e = 5\sigma$, the order of magnitude of positional and orientational FE penalties (as measured from the minimum value) is comparable, so the system spontaneously choses an intermediate state between state (1) and (2).

By setting the inter-particle attraction to a relatively low value ($\varepsilon_{NP,NP} = 0.15$, see Figure 10), it is possible to relax the strong contact constraint. In such a scenario, the particles forgo the energetic advantage of a complete (square-square) contact, and slip along the contact surface. In doing so, the particles reduce the vertical separation between

their centers and, as a result, come closer to the interface-dividing plane. This structure (shown in Figure 12.b) is the basic motif in the superstructure referred to as the Puckered Honeycomb structure.

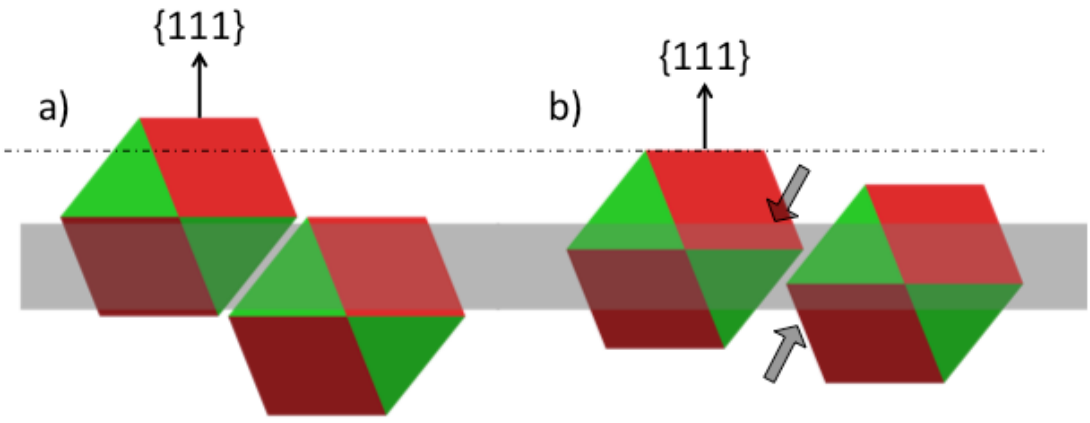

Figure 12: A cartoon representation of two COs at the interface (grey region) with their {111} facets pointing vertically upwards. (a) Situation where the contact between the square faces of the COs is complete. This causes the COs to move away from the interface-dividing plane and out of the interface, which decreases the system's stability; (b) Under specific conditions, the COs can slip along their surface of contact and move into the interface, reducing in the process the vertical separation between their centers of mass.

The strategy developed for modifying the FE for a single particle (section 4.2) can be extended to a two-particle system as follows. For the purpose of stabilizing the Puckered Honeycomb motif, the degree of miscibility between the two fluids ($\varepsilon_{S1,S2}$) can be increased (without changing the relative contact angles of the fluids with the

CO particle). By doing this, the FE well associated with the vertical position becomes shallower, thereby allowing the CO to access a wider range of vertical positions around the interface dividing plane (as shown in section 4.2). Similarly, we can reduce the contact angle between the NP and the top fluid, $\theta_{NP,S1}$ (corresponding to $\varepsilon_{NP,S1}$=0.7) such that the most preferred position is centered about 1.5 - 2.0σ (see Figure 13.a). At this vertical position, the COs preferentially orient themselves with the {110} facet up configuration, with no significant relative separation distance between particle centers. This gives rise to stable linear, rod-like structures (see Figure 13.b.). It is important to note that if $\varepsilon_{NP,S1}$ is increased, $\varepsilon_{NP,NP}$ has to be re-adjusted to mitigate the NP's solvation preference to fluid S1; specifically, if $\varepsilon_{NP,S1}$ is set to 0.7, then $\varepsilon_{NP,NP}$ must be increased from 0.15 to ~0.3.

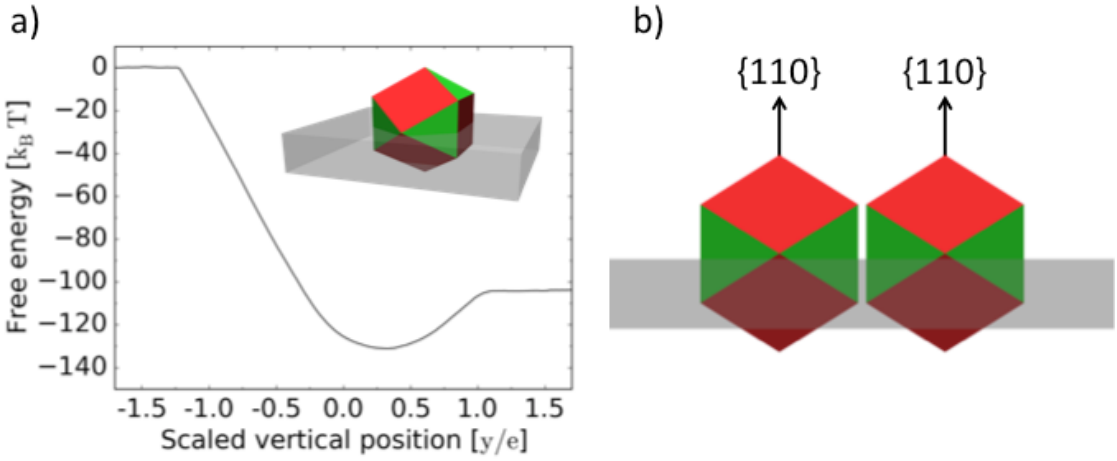

Figure 13: (a) FE profile for a CO (e=5σ) and $\varepsilon_{NP,S1}$ = 0.7. Under these conditions, CO prefers to stay at H~0.4e and with its {110} facet up; (b) Stable rod-like motif formed by two COs. The interfacial region in the snapshots is shown in grey.

4.4 Validity of the Continuum Model

As can be seen in Figs. 6.b and 17.b, the continuum model proposed in Sec. 3 is able to capture semi-quantitatively the key features and trends of behavior of the FE plots for the polybead, solvent explicit model and associated orientational and positional preferences of a single NP at a fluid-fluid interface. Compared to earlier models [24], the continuum model that we propose here gives a more detailed and accurate description of the system when the size of the particle is about one order of magnitude larger than the size of the liquid molecules (O(10)). An elegant feature of this formulation lies in the fact that it reduces to the previous sharp-interface model in the limit of very large particle sizes, as illustarated in Fig. 14. Indeed, when size of the particle is much greater than the width of the interface, we can write:

Excluded volume (V_{ex}) ≈ (Excluded area × interface width)

NP area in contact with the mixing region ≈ (Perimeter × interface width)

As we saw in section 4.1, this continuum model correctly predicts the positional FE minimum for a cube.

Figure 14: Illustration of the idea that if the particle size is much bigger than the characteristic thickness of the interface (as in the rightmost cube), the proposed finite-interface model approaches the sharp-interface model.

As further validation, we generated FE vs H profiles, for a single cube ($e=5\sigma$) at the interface, for different sets of ($\varepsilon_{S1,S2}$, $\varepsilon_{NP,S1}$) values (see Figure 15; top panel). Each profile is represented using the F($\varepsilon_{S1,S2}$, $\varepsilon_{NP,S1}$) notation. Next, we calculated the change in the FE (ΔF) (at corresponding values of H) caused by a change in one parameter at a time. We, then, add the change caused by both parameters individually to the base value (F(0.5,0.5)). It can be seen, in Figure 15 bottom panel, that this sum is equal to the target function (F(0.6,0.6)). This additivity of individual FE effects for the solvent-explicit polybead model is in agreement with the linear structure of the relevant terms in the continuum model formulation [Eq. (4)] ((non-linear effects are absent); namely:

$$F(0.5, 0.5) + [F(0.6, 0.5) - F(0.5, 0.5)] + [F(0.5, 0.6) - F(0.5, 0.5)] = F(0.6, 0.6) \quad (5)$$

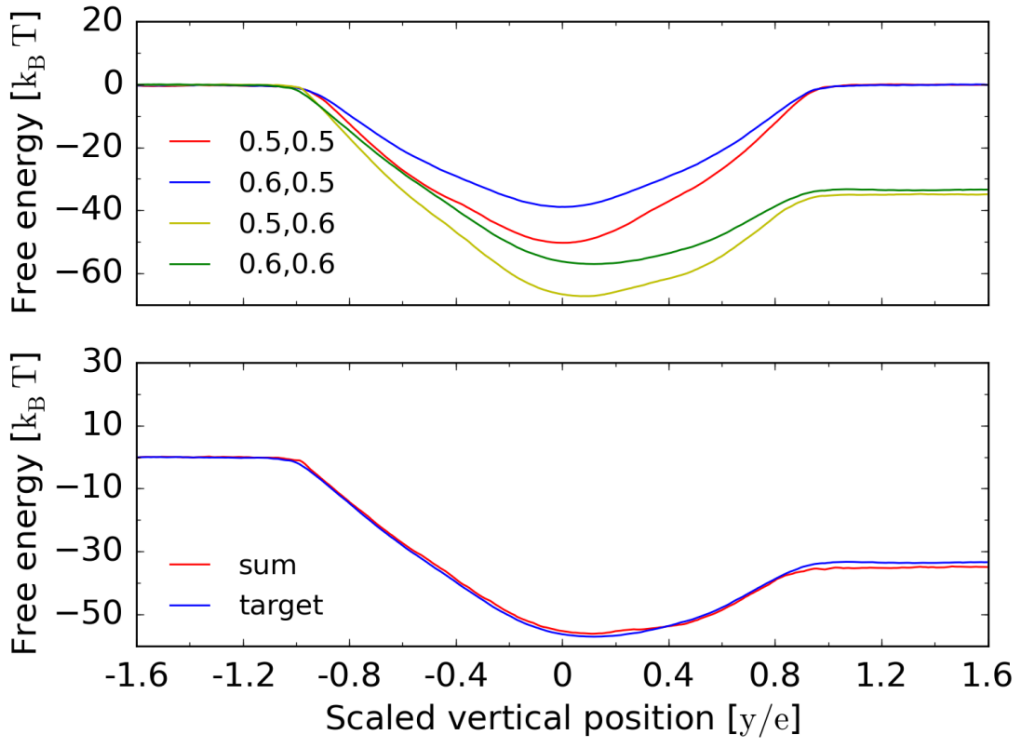

Figure 15: (Top) MD simulation results for a polybead Cube (e=5σ) for different sets of ($\varepsilon_{S1,S2}$, $\varepsilon_{NP,S1}$) parameter values; (Bottom) The sum (red curve) of changes in FE (ΔF) caused by independent changes in parameters to the base FE profile matches with the profile generated by changing both parameters simultaneously (target function, blue curve).

5. CONCLUSIONS

By using a polybead model, we simulated an isolated NP at an explicitly defined fluid-fluid interface. Through the use of biased sampling techniques, we mapped the orientational and positional FE function for a cubic NP. In general, this methodology can be applied to any polyhedral shape (e.g., Fig. 11.a for a CO), provided it can be formed using a polybead model. We found that an isolated cube at the interface, with no selective preference to either fluids, prefers a {111} up orientation. A Pieranski-type formulation[22] of the continuum model presented in refs. [23], [24], however, predicts a {110} up orientation. It was found that when the width of the mixing-region is not negligible relative to the size of the cube, the effect of this finite interface on the underlying FE is significant. The FE trends observed in the MD simulations were justified on the basis of a proposed finite-interface-thickness continuum model. This model enacts the principle of minimization of interfacial energy on the basis of reducing the interfacial volume (i.e. the volume of the mixing region) by maximizing the volume occupied therein by the NP.

Thereafter, we proposed a strategy to gain access to different orientational configurations for a given NP shape. By changing the contact angles between the three system components, we can alter the shape and depth of the FE wells (that govern both positional and orientational behavior) to create conditions at which different target configurations of the NP can be stabilized. We showed that for certain conditions ($\varepsilon_{S1,S2} = 0.6$, $\varepsilon_{NP,S1} = 0.7$) a cube of edge size, $e=5\sigma$ moves away from the

interface-dividing plane and orients with its {100} facet up. We then built upon these principles to explain and control the assembly of two COs. Indeed, we predicted conditions for the stability of different types of assemblies and validated our predictions through direct MD simulations.

We expect that the approaches developed in this study and the results generated therefrom to be potentially translatable to real systems and guide experimental efforts to improve protocols for interfacial assembly of NPs. Although, specific NP materials and

fluids can be approximately mapped into our coarse-grained model by calibrating the different contact angles between the solid and fluid phases, several refinements can be introduced. For example, the NP model can be more detailed by using more numerous beads to represent it surface and even by adding grafted ligands (if existing in the real system). Likewise, more atomistic models could be used to describe specific solvents.

The implicit-solvent continuum model we propose and validate (a clear improvement over a previous sharp-interface theory) is also expected to be valuable tool to model the interfacial behavior of NPs. Through application of this analytical model, one can gain a more complete and intuitive understanding of the underlying physics that govern the relative stability of different NP orientations at various vertical positions. There exist different directions that can be pursued to better characterize the theory. Recently, it was shown[35] that the {111} facet up preference of the cube can be captured by including the effect of capillary deformation in a sharp interface model. It is conjectured that, for small nanoparticles (<10 nm), the dynamic nature of the particle motions

perpendicular to the interface averages this capillary effect into an effective mixing region. Here for example, a more detailed model could be developed by further decoupling the effect of the deformation of the diving-surface in contact with the nanoparticle from the average width of the mixing region. In this context, simulations of nanoparticles of increasing larger sizes (relative to the interface thickness) will also be informative to detect and quantify the contributions of capillary deformations and interfacial mixing.

Future modeling studies could extend our work by probing the effect of NP solvent wetting at a vapor-liquid interface instead of a liquid-liquid interface. Also, multi-particle interfacial assembly behavior can also be studied by using solvent-explicit coarse-grained models or be aided by a solvent-implicit continuum model similar to those presented here. Work along these lines is currently under way.

APPENDIX

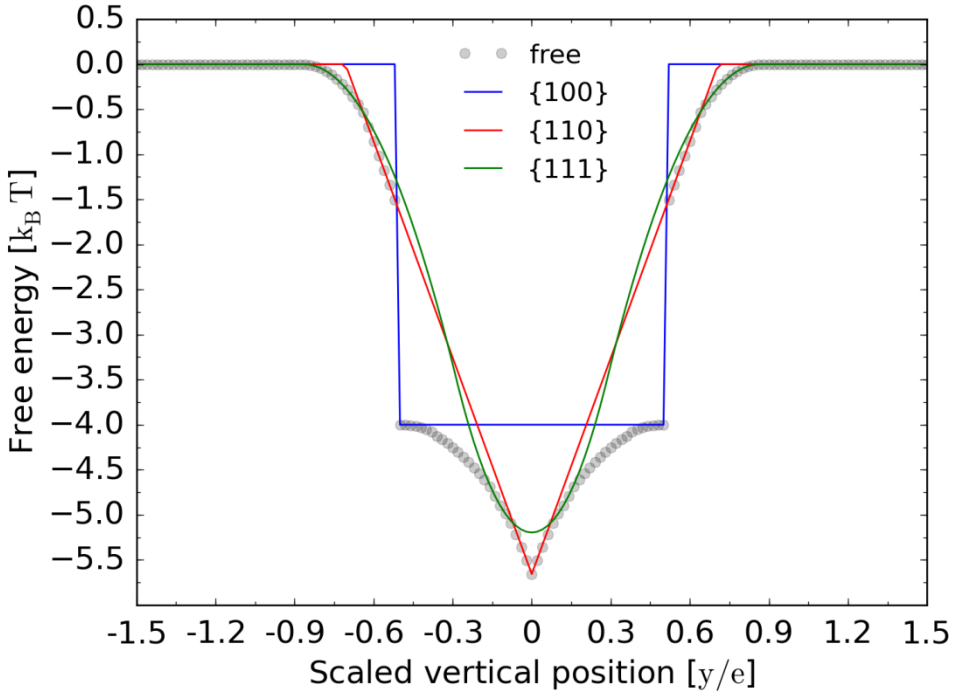

Figure S1: FE vs H for a cube at the base case conditions corresponding to three major orientations (blue, red, and green) and for the most stable orientation envelope (black). Sharp interface theoretical model. Notice that the most preferred orientation is {110}-up.

Basis of the Continuum approximation

The system is divided into a set of adjacently placed, vertical slabs. Each slab contains a slice of the NP based on the values of the parameters (H,θ,ψ). The fluid phase in

the i^{th} slab is characterized by distinct values of the physical properties, β_i and $\gamma_{P,i}$. The energy of the i^{th} slab can then be written as,

$$f_i(H,\theta,\psi) = \gamma_{P,i}A_{P,i} + \beta_i\left(V_i - V_{P,i}\right) \quad \text{(S1)}$$

where $\gamma_{P,i}$ is the interfacial tension between the NP and the fluid phase in the slab, and, β_i is the internal energy per unit volume of fluid phase in the slab. $A_{P,i}$ and $V_{P,i}$ represent the curved surface area and the volume of NP in the slab respectively, and V_i represents the total slab volume. The total potential energy of the system *F* is given by summing the contributions of all individual slabs;

$$F(H,\theta,\psi) = \sum_{i=Bulk\ 1}^{Bulk\ 2} f_i + \text{const} \quad \text{(S2)}$$

F is defined relative to some arbitrary reference energy state. To eliminate the constant from the above expression, we shift the energy state, where the NP is completely immersed in the bulk of fluid 2, to zero:

$$F(\infty) = \gamma_{P,Bulk2}A_P - \beta_{Bulk\ 2}V_P + \sum_{i=Bulk1}^{Bulk\ 2}\beta_i V_i \quad \text{(S3)}$$

where $A_P(=\sum_i A_{P,i})$ and $V_P(=\sum_i V_{P,i})$ refer to the total surface area and the total volume enclosed by the NP shape.

$$\Delta F(H,\theta,\psi) = \sum_{i=Bulk\ 1}^{Bulk\ 2}\left(\gamma_{T,i} - \gamma_{P,\ Bulk2}\right)A_{P,i} + (\beta_{Bulk\ 2} - \beta_i)V_{P,i} \qquad (4)$$

The parameters $\gamma_{P,i}$, β_i are modeled using sigmoidal functions[36], *S*(H,A,H_m,D)* of the same form as shown by the fluid density (Figure 3.a.).

$$S(H,A,H_m,D) = \frac{A}{2}\tanh 2\ \frac{(H-H_m)}{D} \qquad (S4)$$

$$S^*(H,A,H_m,D,W) = S(H,A,(H_m+W),D) + S(H,-A,(H_m-W),D) \qquad (S5)$$

where H is the vertical position from the interface dividing plane, and (A, H_m, D, W) is the set of fitting parameters in eq. S5. We then fit eq. (4) to the results from MD simulations as shown in Figure 6.a. The parameter values, obtained from the fitting operation, are used to generate Figure 6.b. For the base case for a cube of size 5σ, the fitting parameters are A = -0.55, H_m = 0.0, D = 1.24, W = 1.37 for the γ function, and A = -0.15, H_m = 0.0, D = 1.24, W = 1.37 for the β function.

REFERENCES

[1] W. J. Baumgardner, K. Whitham, and T. Hanrath, “Confined-but-Connected Quantum Solids via Controlled Ligand Displacement,” *Nano Lett.*, vol. 13, no. 7, pp. 3225–3231, Jul. 2013.

[2] W. H. Evers, B. Goris, S. Bals, M. Casavola, J. de Graaf, R. V. Roij, M. Dijkstra, and D. Vanmaekelbergh, “Low-Dimensional Semiconductor Superlattices Formed by Geometric Control over Nanocrystal Attachment,” *Nano Lett.*, vol. 13, no. 6, pp. 2317–2323, Jun. 2013.

[3] S. Dasgupta, M. Katava, M. Faraj, T. Auth, and G. Gompper, “Capillary Assembly of Microscale Ellipsoidal, Cuboidal, and Spherical Particles at Interfaces,” *Langmuir*, vol. 30, no. 40, pp. 11873–11882, Oct. 2014.

[4] W. van der Stam, A. P. Gantapara, Q. A. Akkerman, G. Soligno, J. D. Meeldijk, R. van Roij, M. Dijkstra, and C. de Mello Donega, “Self-Assembly of Colloidal Hexagonal Bipyramid- and Bifrustum-Shaped ZnS Nanocrystals into Two-Dimensional Superstructures,” *Nano Lett.*, vol. 14, no. 2, pp. 1032–1037, Feb. 2014.

[5] E. Kalesaki, W. H. Evers, G. Allan, D. Vanmaekelbergh, and C. Delerue, “Electronic structure of atomically coherent square semiconductor superlattices with dimensionality below two,” *Phys. Rev. B*, vol. 88, no. 11, p. 115431, Sep.

2013.

[6] P. O. Anikeeva, J. E. Halpert, M. G. Bawendi, and V. Bulović, “Quantum Dot Light-Emitting Devices with Electroluminescence Tunable over the Entire Visible Spectrum,” *Nano Lett.*, vol. 9, no. 7, pp. 2532–2536, Jul. 2009.

[7] P.-P. Fang, S. Chen, H. Deng, M. D. Scanlon, F. Gumy, H. J. Lee, D. Momotenko, V. Amstutz, F. Cortés-Salazar, C. M. Pereira, Z. Yang, and H. H. Girault, “Conductive Gold Nanoparticle Mirrors at Liquid/Liquid Interfaces,” *… nano*, Oct. 2013.

[8] L Mangolini, A. E Thimsen, and U. Kortshagen, “High-Yield Plasma Synthesis of Luminescent Silicon Nanocrystals,” *Nano Lett.*, Mar. 2005.

[9] J. Baxter, Z. Bian, G. Chen, D. Danielson, M. S. Dresselhaus, A. G. Fedorov, T. S. Fisher, C. W. Jones, E. Maginn, U. Kortshagen, A. Manthiram, A. Nozik, D. R. Rolison, T. Sands, L. Shi, D. Sholl, and Y. Wu, “Nanoscale design to enable the revolution in renewable energy,” *Energy & Environmental Science*, vol. 2, no. 6, pp. 559–588, 2009.

[10] A. J. Nozik, M. C. Beard, J. M. Luther, M. Law, R. J. Ellingson, and J. C. Johnson, “Semiconductor Quantum Dots and Quantum Dot Arrays and Applications of Multiple Exciton Generation to Third-Generation Photovoltaic Solar Cells,” *Chemical …*, Oct. 2010.

[11] D. V. Talapin, J.-S. Lee, M. V. Kovalenko, and E. V. Shevchenko, “Prospects of Colloidal Nanocrystals for Electronic and Optoelectronic Applications,” *Chemical*

…, Dec. 2009.

[12] Z.-Y. Zhou, N. Tian, J.-T. Li, I. Broadwell, and S.-G. Sun, “Nanomaterials of high surface energy with exceptional properties in catalysis and energy storage,” *Chemical Society Reviews*, vol. 40, no. 7, pp. 4167–4185, 2011.

[13] G. W. Crabtree and J. L. Sarrao, “Opportunities for mesoscale science,” *MRS Bulletin*, vol. 37, no. 11, pp. 1079–1088, Nov. 2012.

[14] U. Agarwal, F. A. Escobedo, “Mesophase behaviour of polyhedral particles,” *Nature Publishing Group*, vol. 10, no. 3, pp. 230–235, Feb. 2011.

[15] P. F. Damasceno, M. Engel, and S. C. Glotzer, “Predictive Self-Assembly of Polyhedra into Complex Structures,” *Science*, vol. 337, no. 6093, pp. 453–457, Jul. 2012.

[16] V. Thapar, T. Hanrath, and F. A. Escobedo, “Entropic self-assembly of freely rotating polyhedral particles confined to a flat interface,” *Soft Matter*, vol. 11, pp. 1481–1491, Feb. 2015.

[17] A. P. Gantapara, J. de Graaf, R. van Roij, and M. Dijkstra, “Phase Diagram and Structural Diversity of a Family of Truncated Cubes: Degenerate Close-Packed Structures and Vacancy-Rich States,” *Phys. Rev. Lett.*, vol. 111, no. 1, pp. 015501–5, Jul. 2013.

[18] S. Razavi, J. Koplik, and I. Kretzschmar, “The effect of capillary bridging on the Janus particle stability at the interface of two immiscible liquids,” *Soft Matter*, vol. 9, no. 18, pp. 4585–5, 2013.

[19] H.-M. Gao, Z.-Y. Lu, H. Liu, Z.-Y. Sun, and L.-J. An, “Orientation and surface activity of Janus particles at fluid-fluid interfaces,” *J. Chem. Phys.*, vol. 141, no. 13, pp. 134907–10, Oct. 2014.

[20] W. Ramsden, “Separation of Solids in the Surface-Layers of Solutions and ‘Suspensions’ (Observations on Surface-Membranes, Bubbles, Emulsions, and Mechanical Coagulation). -- Preliminary Account,” *Proceedings of the Royal Society of London*, vol. 72, pp. 156–164 IS –, 1903.

[21] S. U. Pickering, “CXCVI.—Emulsions,” *J. Chem. Soc., Trans.*, vol. 91, no. 0, pp. 2001–2021, 1907.

[22] P. Pieranski, “Two-Dimensional Interfacial Colloidal Crystals,” *Phys. Rev. Lett.*, vol. 45, no. 7, pp. 569–572, Aug. 1980.

[23] J. de Graaf, M. Dijkstra, and R. van Roij, “Triangular tessellation scheme for the adsorption free energy at the liquid-liquid interface: Towards nonconvex patterned colloids,” *Phys. Rev. E*, vol. 80, no. 5, p. 051405, Nov. 2009.

[24] J. de Graaf, M. Dijkstra, and R. van Roij, “Adsorption trajectories and free-energy separatrices for colloidal particles in contact with a liquid-liquid interface,” *J. Chem. Phys.*, vol. 132, no. 16, p. 164902, Apr. 2010.

[25] M. R. Khadilkar and F. A. Escobedo, “Self-assembly of binary space-tessellating compounds,” *J. Chem. Phys.*, vol. 137, no. 19, p. 194907, Nov. 2012.

[26] S. Plimpton, “Fast Parallel Algorithms for Short-Range Molecular Dynamics,” *Journal of Computational Physics*, vol. 117, no. 1, pp. 1–19, 1995.

[27] D. Duque, J. C. Pàmies, and L. F. Vega, “Interfacial properties of Lennard-Jones chains by direct simulation and density gradient theory,” *J. Chem. Phys.*, vol. 121, no. 22, pp. 11395–11401, Dec. 2004.

[28] E. S. Savoy and F. A. Escobedo, “Molecular Simulations of Wetting of a Rough Surface by an Oily Fluid: Effect of Topology, Chemistry, and Droplet Size on Wetting Transition Rates,” *Langmuir*, vol. 28, no. 7, pp. 3412–3419, Feb. 2012.

[29] G. M. Torrie and J. P. Valleau, “Nonphysical sampling distributions in Monte Carlo free-energy estimation: Umbrella sampling,” *Journal of Computational Physics*, vol. 23, no. 2, pp. 187–199, Feb. 1977.

[30] S. Kumar, J. M. Rosenberg, D. Bouzida, R. H. Swendsen, and P. A. Kollman, “THE weighted histogram analysis method for free-energy calculations on biomolecules. I. The method,” *J. Comput. Chem.*, vol. 13, no. 8, pp. 1011–1021, Oct. 1992.

[31] J. de Graaf, M. Dijkstra, and R. van Roij, “Triangular tessellation scheme for the adsorption free energy at the liquid-liquid interface: Towards nonconvex patterned colloids,” *Phys. Rev. E*, vol. 80, no. 5, pp. 051405–19, Nov. 2009.

[32] J. J. Choi, K. Bian, W. J. Baumgardner, D.-M. Smilgies, and T. Hanrath, “Interface-Induced Nucleation, Orientational Alignment and Symmetry Transformations in Nanocube Superlattices,” *Nano Lett.*, vol. 12, no. 9, pp. 4791–4798, Aug. 2012.

[33] M. Meyer, M. Mareschal, and M. Hayoun, “Computer modeling of a liquid–liquid interface,” *The Journal of chemical …*, vol. 89, no. 2, p. 1067, 1988.

[34] D. Chandler, J. D. Weeks, and H. C. Andersen, “Van der Waals picture of liquids, solids, and phase transformations,” *Science*, 1983.

[35] G. Soligno, M. Dijkstra, and R. van Roij, “Self-Assembly of Cubes into 2D Hexagonal and Honeycomb Lattices by Hexapolar Capillary Interactions,” *Phys. Rev. Lett.*, vol. 116, no. 25, pp. 258001–6, Jun. 2016.

[36] K. G. Weil, “J. S. Rowlinson and B. Widom: Molecular Theory of Capillarity, Clarendon Press, Oxford 1982. 327 Seiten, Preis: £ 30,–.,” *Berichte der Bunsengesellschaft für physikalische Chemie*, vol. 88, no. 6, pp. 586–586, Jun. 1984.